Applied Energy 203 (2017) 959–971

Contents lists available at ScienceDirect

Applied Energy

journal homepage: www.elsevier.com/locate/apenergy

Optimized dispatch in a first-principles concentrating solar power production model

Michael J. Wagner [a], Alexandra M. Newman [b,*], William T. Hamilton [b], Robert J. Braun [b]

[a] National Renewable Energy Laboratory, Thermal Systems Group, 15013 Denver West Parkway, Golden, CO 80401, United States
[b] Colorado School of Mines, Department of Mechanical Engineering, 1500 Illinois Street, Golden, CO 80401, United States

HIGHLIGHTS

- A profit maximizing solution operates concentrated solar power towers.
- Dispatch optimization integrates a techno-economic analysis tool.
- An optimized strategy improves plant profitability by 5–20%.
- Further improvements derive from a reduction in the number of cycles by 50%.
- Power cycle start-ups reduce from 370 to 250 per year without affecting energy output.

ARTICLE INFO

Article history:
Received 25 November 2016
Received in revised form 18 June 2017
Accepted 19 June 2017

Keywords:
Dispatch optimization
Grid integration
Concentrating Solar Power (CSP)
Thermal energy storage
Mixed-integer linear programming
Systems analysis

ABSTRACT

Concentrating solar power towers, which include a steam-Rankine cycle with molten salt thermal energy storage, is an emerging technology whose maximum effectiveness relies on an optimal operational and dispatch policy. Given parameters such as start-up and shut-down penalties, expected electricity price profiles, solar availability, and system interoperability requirements, this paper seeks a profit-maximizing solution that determines start-up and shut-down times for the power cycle and solar receiver, and the times at which to dispatch stored and instantaneous quantities of energy over a 48-h horizon at hourly fidelity. The mixed-integer linear program (MIP) is subject to constraints including: (i) minimum and maximum rates of start-up and shut-down, (ii) energy balance, including energetic state of the system as a whole and its components, (iii) logical rules governing the operational modes of the power cycle and solar receiver, and (iv) operational consistency between time periods.

The novelty in this work lies in the successful integration of a dispatch optimization model into a detailed techno-economic analysis tool, specifically, the National Renewable Energy Laboratory's *System Advisor Model* (SAM). The MIP produces an optimized operating strategy, historically determined via a heuristic. Using several market electricity pricing profiles, we present comparative results for a system with and without dispatch optimization, indicating that dispatch optimization can improve plant profitability by 5–20% and thereby alter the economics of concentrating solar power technology. While we examine a molten salt power tower system, this analysis is equally applicable to the more mature concentrating solar parabolic trough system with thermal energy storage.

© 2017 Elsevier Ltd. All rights reserved.

1. Background

The ability of renewable energy to be dispatched flexibly enables significant market penetration compared to renewable energy systems that are highly variable (e.g., wind) and/or that lack associated storage systems (e.g., photovoltaics without storage). We examine one type of solar technology, concentrating solar power (CSP), that manifests itself as: parabolic trough, linear fresnel, dish stirling, and power tower. The latter, and the one

Abbreviations: CSP, Concentrating Solar Power; HTF, Heat Transfer Fluid; MIP, Mixed-Integer Linear Program; MSPT, Molten Salt Power Tower; PPA, Power Purchase Agreement; SAM, System Advisor Model; TES, Thermal Energy Storage; TOD, Time-of-Dispatch.

* Corresponding author.
E-mail addresses: michael.wagner@nrel.gov (M.J. Wagner), anewman@mines.edu (A.M. Newman), whamilton@mines.edu (W.T. Hamilton), rbraun@mines.edu (R.J. Braun).

http://dx.doi.org/10.1016/j.apenergy.2017.06.072
0306-2619/© 2017 Elsevier Ltd. All rights reserved.

addressed in this paper, is thought to possess the most significant potential for improvements in efficiencies and reductions in cost [1]. Concentrating solar power tower technology uses thousands of sun-tracking mirrors (heliostats) that focus on a central receiver to heat molten salt to temperatures above 565°C (1050°F). The molten salt can then be pumped to a power cycle to generate electricity or efficiently stored for use when sunlight is not available [2]. However, the economic viability and widespread implementation of CSP technologies are strongly tied to their ability to extend their diurnal operational characteristics across peak demand time periods and during periods when solar energy is curtailed due to the sun setting or cloud cover [3]. Thermal energy storage (TES) is an enabling technology which can amass the energy captured by the receiver as a reserve for dispatch at a later, more economical time. In fact, TES integration enables CSP to be a dispatchable renewable resource whose economics are enhanced by both improved utilization of the power cycle and an ability to shift power production to better coincide with peak demands and high-value-electricity time periods [4].

High-temperature molten salt TES has been successfully implemented in CSP tower systems [5,6] and in parabolic trough systems, the latter in an *indirect* manner through use of an intermediate oil-to-molten salt heat exchanger. So-called *direct* TES systems such as the power tower technology use molten salt both as the storage medium and as the heat transfer fluid in the receiver, thereby avoiding the intermediate heat exchanger and improving system efficiency and dispatchability [7].

The maximum storage capacity of the TES system is determined during a plant design process that considers several factors including the thermal power rating of the solar field and power cycle subsystems, plant location, project economics, and the desired *capacity factor*, which is defined as the quotient of total annual electrical energy production and the electrical energy production should the plant operate continuously at rated power output. Thermal energy storage sizing also depends on the operational scheme. For example, a plant that intends to operate primarily during high-revenue morning or evening periods while reducing production during daylight hours requires more TES capacity than a plant with an identical capacity factor that generates power during all daylight hours. CSP plants that target dispatch during high-revenue periods operate differently than those that minimize the average cost of energy. The former relies more extensively on a carefully planned dispatch schedule that anticipates the timing and level of thermal power production in the solar field, energy consumption for receiver and plant start up, and the charge state of TES over time. Formal optimization methods can determine the dispatch profile that maximizes electricity sales revenue over a particular time horizon given a specific system configuration, expected solar resource, pricing or time-of-dispatch (TOD) profile, and operational constraints – a process referred to as *dispatch optimization.*

The intelligent dispatch of stored energy can greatly enhance the value of electricity by providing firm capacity and ancillary services, and by generating electricity during time periods in which rates are especially high [8]. Dispatch optimization involves the manipulation of the timing and rate at which electricity is generated by the power cycle and captures both physical processes and time [9]. This paper presents a methodology, implementation, and publicly available tool for simulating CSP power tower systems with optimized dispatch. The method expands on previous work by directly incorporating formal optimization techniques into the SAM [10] simulation software, for which previous research has relied on heuristics or on optimizing dispatch using simulation output *a posteriori* as optimization model input. SAM assesses CSP performance, simulating renewable technologies including CSP, wind, geothermal, photovoltaic, biomass, solar hot water, and generic systems. The software is free to download and use, and the tools developed in the current work are freely available [11]. Each technology can be paired with a financial model to evaluate the economic performance of a project within particular market, incentive, and cost environments.

1.1. Related work

Optimization modeling has been applied to many types of energy systems, e.g., [9] who retrofit an existing building and determine a corresponding dispatch strategy, and [12] who examine multiple objectives in optimizing stand-alone hybrid energy systems, also with the corresponding dispatch. Other authors examine only dispatch, e.g., [13], who apply a simulation model to a hybrid photovoltaic and tri-generation power system to decrease waste from excess heat, while [14] formulate an optimization model (a mixed-integer linear program, like ours) that combines both dispatchable and intermittent power, the latter as a result of a virtual plant, to maximize profits. Similarly, [15] develop an optimization model that dispatches wind, but, in contrast to the previous work, theirs focuses on minimizing active power losses in the system while constraining reactive power; the model is solved heuristically. Thorin et al. [16–18] operate in a market environment (as does [14]), the former for a unit commitment problem, applying an exact approach (i.e., Lagrangian Relaxation) to a mixed-integer program; Cho et al. [17] optimize a combined cooling, heating, and power system to optimize the tradeoffs between system cost, energy production and emissions, and test their model on a variety of geographic sites in the U.S. with differing weather conditions; Fürsch et al. [18] examine the expansion of a power network and the corresponding dispatch strategies in Europe; using an optimization model which combines both investment and dispatch decisions, they conclude that even optimal grid extensions, coupled with capital cost reductions for renewable technologies, leads to significantly higher overall average electricity system costs over a time horizon of three to four decades. Parisio et al. [19] use model predictive control within an optimization (mixed-integer programming) framework in which the goal is to minimize costs subject to microgrid system constraints such a capacities, minimum up- and down-times, and start-up and shut-down requirements. They test instances of their model on an experimental microgrid in Greece. Zheng et al. [20] provide a review of bio-inspired optimization of sustainable energy systems. These works examine problems similar to ours in that dispatch policies are considered, some even using the mathematical framework in this paper. However, none of these examines concentrating solar power in particular, with its own sets of objectives and rules. We next discuss the research specific to power tower technology.

Simulation is used to predict the total electrical energy production from an existing or previously designed CSP plant over its lifetime in order to evaluate the financial return on investment, the cost of energy, the environmental (mitigation) impact, or some other measure of interest. The standard method for CSP simulation requires calculation of plant behavior over a time horizon (typically, one year with one-hour time steps) [21], and it develops a picture of long-term energy production by sequentially modeling performance at relatively short time steps compared to the overall time window of interest (e.g., hourly calculations to establish lifetime metrics). CSP systems are primarily constrained by immediate concerns, such as component or subsystem operational states, conservation of mass and energy, and heat transfer, thermodynamic, or thermo-mechanical principles.

The previous dispatch approach implemented in SAM uses a simple heuristic that allows the user to specify requirements before thermal storage can be dispatched; this heuristic does not

consider the expected *future* thermal energy production, TES charge state, or price at which electricity can be sold, but instead determines the operational state of the power cycle based on the current TES charge state and the hour of the day. The heuristic can improve plant production during high-value hours as exemplified by SAM or Guédez et al. [22], but can ultimately decrease the utilization of the solar field throughout the year because of TES over-charge situations.

By contrast, this work adopts a formal approach by formulating the problem as a mixed-integer program (MIP) that leverages state-of-the-art modeling languages and solvers ([23,24]) to make the solution of a mathematical problem containing thousands of variables and constraints tractable.

Madaeni et al. [25] present a simplified approach for determining an optimal dispatch profile while implementing MIP techniques. The authors use SAM to generate an hourly thermal power production profile throughout the year that is considered as fixed input to the MIP model originally outlined in [26]. This approach factors in the simulated performance of the solar field, but omits interactions between the solar field and thermal storage or the power cycle. The latter subsystems are modeled as part of a MIP that determines the TES state of charge and electricity production from the cycle. This method improves tractability by reserving the detailed model to generate fixed input while utilizing a simplified energy balance model to characterize TES charge and power cycle generation. Furthermore, [25] employ a rolling time horizon methodology in which they consider a 48-h time horizon, updated every 24 h. Our work largely adopts this approach, but importantly, uses the optimized schedule to control operational decisions within SAM's detailed simulation model, whereas the work of [25] uses the results from the MIP as the actual estimate of plant production throughout the year.

1.2. Goals of the current work

Dispatch optimization improves the profitability of existing or planned CSP facilities, but it is also of great interest to policymakers and researchers who seek to better understand the projected performance of CSP systems under various deployment and grid operations scenarios. However, previous work (cf. [8,25,26]) considers dispatchability from the perspective of grid integration in which CSP systems are designed at an energy-flow and system sizing level to assess suitability for meeting grid and market demands. The contribution of our work is its evaluation of the relationship between optimal dispatch profiles and technology design. Accordingly, this work fills the gap between *prescriptive* grid-level models on the one hand that indicate desired technology performance subject to high-level operational requirements (e.g., plant start-up, maximum energy generation) and *descriptive* performance simulations on the other hand whose primary concern is to dynamically synthesize expected plant productivity and financial return given specific component or subsystem thermo-mechanical performance expectations. SAM develops these estimates using annual "macro-simulations" that consist of thousands of sequential "micro-simulations" within a time series, and the plant behavior at any given time step may depend on the state of the system in the previous time step(s). The SAM molten salt power tower (MSPT) model is configured as illustrated in Fig. 1.

The MIP in SAM operates under the following assumptions: (i) solar field thermal production over time is calculated using a simplified "forecast" model and provided as a fixed input to the dispatch model, and (ii) power cycle efficiency depends linearly on thermal input to the cycle and on the ambient temperature, and these efficiency corrections can be implemented as independent terms (see Section 3). Dispatch optimization enables investigation of detailed plant performance issues that are too complex to be easily represented in an energy-balance MIP model. For example, the mechanical stress associated with frequent thermal cycling of power generation equipment may lead to an increase in the frequency of required maintenance [27]. A detailed model can capture these thermo-mechanical impacts when the plant control is influenced by optimized dispatch scheduling.

1.3. Operating considerations

The plant dispatch schedule determines the timing and production level from the power cycle (turbine, generator, condenser, and associated equipment). During operation, the power cycle consumes stored thermal energy from the TES system. Thermal energy storage is charged using high-grade thermal energy that is generated by the solar field during daytime operation, and energy generation is affected by the optical and thermal efficiency of the solar field, by the intensity of the available solar resource, and by the operational state of the solar field. Receiver and power cycle start-up sequences are not necessarily coordinated, so both systems may operate independently with shared interest only in the energy state of the TES system. In some cases, the receiver must curtail energy generation to avoid over-charging thermal storage (thus wasting solar energy).

Before the power cycle or receiver can produce electricity or thermal energy, respectively, start-up requirements must be satisfied, including both a minimum start-up period and a minimum energy state requirement which are surrogates for temperature considerations. In the latter case, the plant equipment cools during shutdown periods and must overcome the system's thermal inertia to begin generating steam that powers the turbine. Likewise, the receiver consumes energy as it heats up and must complete a start-up procedure before producing useful thermal energy. Furthermore, turbine and heat exchanger equipment manufacturers limit the maximum rate of temperature increase during start-up to avoid thermal stress and mechanical failure risks. Both the energy and duration start-up requirements must be met before equipment can begin producing power. These requirements are implemented as a constraint on the maximum energy delivered for start-up during any given time period. Although the duration of start-up must last for at least a minimum number of time steps, longer start-up durations are allowed in practice based on energy availability, and the model must provide this flexibility.

Two start-up scenarios are possible for the power cycle: (i) *cold start-up*, which occurs when the power cycle has shut down for any period of time and seeks to restart; and (ii) *hot start-up*, which occurs when the power cycle has been in *standby* mode and seeks to restart. Cold start-up requires an additional energy contribution and incurs more component wear and tear, whereas hot start-up can happen immediately (from the perspective of the hourly model).

Standby is a mode of operation in which a small (but non-trivial) amount of thermal energy is consumed during each time period to maintain the power cycle and/or receiver equipment in a hot state, ready to quickly ramp up for electricity generation; however, no electricity is produced in standby mode. Consequently, maintaining the power cycle in standby mode is of value if multiple start-up cycles are anticipated over a relatively short time span, or if the energy penalty or ramp rate requirement for start-up is sufficiently severe to justify the small rate of energy consumption by the power cycle.

The receiver can also operate in a standby mode during cloudy periods to avoid the full start-up procedure. In standby, salt from the cold storage tank is pumped through the receiver, and the flow is diverted back into the cold tank where the fluid temperature can decay at a rate that corresponds to the thermal losses from the receiver. Finally, the model accounts for receiver shutdown energy

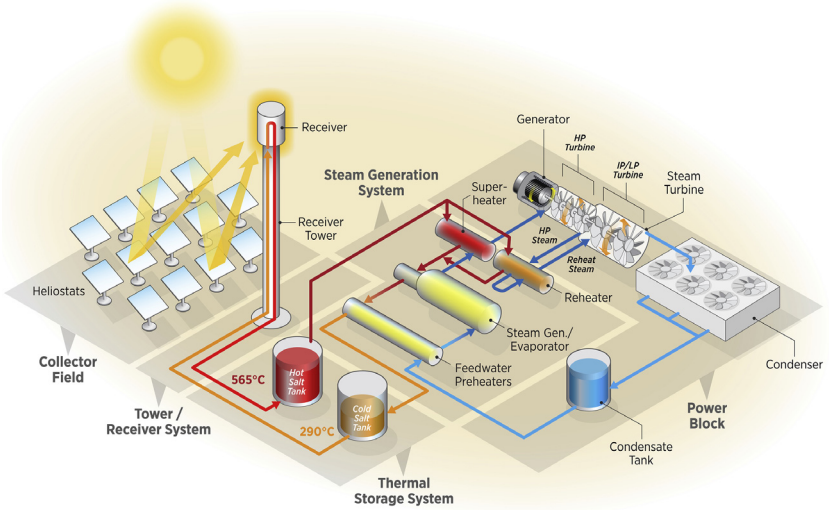

Fig. 1. Molten Salt Power Tower system configuration that is modeled in SAM. The system consists of a heliostat field, molten salt receiver, direct TES system, steam generation system, Rankine power cycle, and heat rejection system (Graphic © NREL/Al Hicks).

consumption in which the heliostat field provides sufficient energy to allow the salt to drain out without freezing before the solar field ends operation for the day. The draining procedure requires approximately fifteen minutes while sunlight is still available, and this effect is modeled as the consumption of 25% of the hourly energy used at the minimum receiver production rate.

2. Mathematical formulation

The parameters, sets, variables, objective function, and constraining relationships are described in this section. The model takes the parameters and sets as given and determines values for the decision variables to maximize an objective function while adhering to the constraints. Some parameters and all variables are subscripted with time t, indicating the time-varying nature of the decisions.

2.1. Parameters and sets

The following MIP, $(\mathcal{R})$, requires the initial operational state of the system, the collector field and receiver energy generation profile, the expected cycle conversion efficiency profile as a function of ambient temperature and thermal input, and the energy price or tariff profile (Table 1). (Initialization parameters used to set variable values at $t = 0$ follow variable notation and are not included here.)

2.2. Variables

The variables (see Table 2) describe energy (thermal kW_t-hr or electric kW_e-hr) states and power flows (thermal kW_t or electric kW_e) in the system. Note that there is a one-to-one conversion between kW_t and kW_e units. Continuous variables "x," "$\dot{w}$," "u," and "s" representing power and energy relate to the receiver, power cycle, and TES. Binary variables "y" enforce operational modes and sequencing such that start-up must occur before normal operation, for example.

2.3. Objective function

The objective maximizes electricity sales, which are represented as the summation over time of the product of electricity price and power generation less parasitic losses. Cost penalties associated with cycle start-up, receiver start-up, and change in electricity production between time steps are subtracted from the revenue.

$$
\begin{aligned}
(\mathcal{R})\ \text{maximize}\quad & \sum_{t\in\mathcal{T}}\Big[\Delta\cdot P_t\Big(\gamma_t(1-\eta_t^c)\dot{w}_t - L^r(x_t^r + x_t^{rsu} + Q^{rl}y_t^{rsb}) - L^c x_t - \dot{W}^h y_t^r \\
& -\dot{W}^b y_t^{csb} - (\dot{W}^{rsb} + E^{hs}/\Delta)y_t^{rsu} - E^{hs}/\Delta\cdot y_t^{rsb} - E^{hs}/\Delta\cdot y_t^{rsd}\Big) \\
& -\gamma_t(C^{rsu}y_t^{rsup} + C^{rhs}y_t^{rhsp}) \\
& -\gamma_t(C^{csu}y_t^{csup} + C^{chs}y_t^{chsp} + \alpha y_t^{csd} + C^{\delta W}\dot{w}_t^{\delta}) + \gamma_t(\overline{P}\Delta x_t^r + \alpha y_t^r)\Big]
\end{aligned}
\tag{1}
$$

2.4. Constraints

The relationships among the variables and parameters are established with a set of simultaneous equations and inequalities. These constraints are presented below topically with a brief description.

2.4.1. Receiver operations

Receiver operations constraints include:

Receiver Start-up

$$u_t^{rsu} \leqslant u_{t-1}^{rsu} + \Delta\cdot x_t^{rsu} \quad \forall t\in\mathcal{T} : t \geqslant 2 \tag{2a}$$
$$u_t^{rsu} \leqslant E^r y_t^{rsu} \quad \forall t\in\mathcal{T} \tag{2b}$$
$$y_t^r \leqslant \frac{u_t^{rsu}}{E^r} + y_{t-1}^r \quad \forall t\in\mathcal{T} : t \geqslant 2 \tag{2c}$$
$$y_t^{rsu} + y_{t-1}^r \leqslant 1 \quad \forall t\in\mathcal{T} : t \geqslant 2 \tag{2d}$$
$$x_t^{rsu} \leqslant Q^{ru} y_t^{rsu} \quad \forall t\in\mathcal{T} \tag{2e}$$
$$\text{if } Q_t^{in} = 0 \text{ then: } y_t^{rsu} = 0 \quad \forall t\in\mathcal{T} \tag{2f}$$

Receiver Supply and Demand

$$x_t^r + x_t^{rsu} + Q^{rsd}y_t^{rsd} \leqslant Q_t^{in} \quad \forall t\in\mathcal{T} \tag{3a}$$
$$x_t^r \leqslant Q_t^{in} y_t^r \quad \forall t\in\mathcal{T} \tag{3b}$$
$$x_t^r \geqslant Q^{rl} y_t^r \quad \forall t\in\mathcal{T} \tag{3c}$$
$$\text{if } Q_t^{in} = 0 \text{ then: } y_t^r = 0 \quad \forall t\in\mathcal{T} \tag{3d}$$

Table 1
Parameters and sets used in ($\mathcal{R}$).

Symbol	Units	Description
Sets		
$\mathcal{T}$		Set of all time steps in the time horizon, $T = \lvert\mathcal{T}\rvert$
Time-indexed parameters		
Q_t^{in}	kW_t	* Energy generated by the solar field in time t
P_t	$/$kW_e$-hr	Electricity sales price in time t
$\dot{W}_t^{net}$	kW_e	Net power production upper limit in time t
$\dot{W}_t^{min}$	kW_e	Minimum *net* power production in time t
η_t^c	–	Normalized condenser parasitic loss in time t
γ_t	–	Exponential time weighting factor; $\Gamma^{(t)}$, where $\Gamma \approx 0.99$
Δ_t^{rs}	–	* Estimated fraction of time step t used for receiver start-up
η_t^{amb}	–	Cycle efficiency adjustment factor in time t
Steady-state parameters		
$\overline{P}$	–	Mean sales price ($/kW$_e$-hr); $\sum_{t\in\mathcal{T}} P_t/T$
η^{des}	–	Cycle nominal efficiency
η^p	–	* Slope of linear approximation of power cycle performance curve
τ	hr	Frequency of optimization problem execution
E^u	kW_t-hr	Energy storage capacity
E^r	kW_t-hr	Required energy consumed to start receiver
E^c	kW_t-hr	Required energy consumed to start cycle
E^{hs}	kW_t-hr	Heliostat field startup or shutdown parasitic loss
W^u	kW_e	Cycle electric power rated capacity
W^l	kW_e	Minimum electric power output from cycle
$\dot{W}^h$	kW_e	Heliostat field tracking parasitic loss
$\dot{W}^b$	kW_e	Power cycle standby operation parasitic load
$\dot{W}^{rsb}$	kW_e	Tower piping heat trace parasitic loss
Q^u	kW_t	Cycle thermal power capacity
Q^l	kW_t	Minimum operational thermal power input to cycle
Q^{ru}	kW_t	Allowable power per period for receiver start-up
Q^{rl}	kW_t	Minimum operational thermal power delivered by receiver
Q^{rsd}	kW_t	Required thermal power for receiver shut-down
Q^{rsb}	kW_t	Required thermal power for receiver standby
Q^c	kW_t	Allowable power per period for cycle start-up
Q^b	kW_t	Standby thermal power consumption per period
L^r	kW_e/kW_t	Receiver pumping power per unit power produced
L^c	kW_e/kW_t	Cycle Heat Transfer Fluid (HTF) pumping power per unit energy consumed
C^{rsu}	$	Penalty for receiver start-up (from 0)
C^{rhs}	$	Penalty for receiver start-up (from hot standby)
C^{csu}	$	Penalty for cycle start-up (from 0)
C^{chs}	$	Penalty for cycle start-up (from hot idle)
$C^{\delta W}$	$/$kW_e$	Penalty for any positive change in electricity production
Δ	hr	Time step duration
Δ^l	hr	Minimum duration of receiver start-up in period
α	$	Conversion factor between unit-less and monetary values
$\mathbb{M}$		A sufficiently large number

* Parameter is calculated from fixed input and discussed below.

Logic Governing Receiver Modes

$$y_t^{rsu} + y_t^{rsb} \leqslant 1 \quad \forall t \in \mathcal{T} \tag{4a}$$
$$y_t^{r} + y_t^{rsb} \leqslant 1 \quad \forall t \in \mathcal{T} \tag{4b}$$
$$y_t^{rsb} \leqslant y_{t-1}^{r} + y_{t-1}^{rsb} \quad \forall t \in \mathcal{T} : t \geqslant 2 \tag{4c}$$
$$y_t^{rsup} \geqslant y_t^{rsu} - y_{t-1}^{rsu} \quad \forall t \in \mathcal{T} : t \geqslant 2 \tag{4d}$$
$$y_t^{rhsp} \geqslant y_t^{r} - (1 - y_{t-1}^{rsb}) \quad \forall t \in \mathcal{T} : t \geqslant 2 \tag{4e}$$
$$y_{t-1}^{rsd} \geqslant (y_{t-1}^{r} - y_t^{r}) + (y_{t-1}^{rsb} - y_t^{rsb}) \quad \forall t \in \mathcal{T} : t \geqslant 2 \tag{4f}$$

($\mathcal{R}$) considers receiver start-up inventory and the criteria that must be satisfied in order for it to produce useful power. Constraint (2a) tracks start-up energy "inventory" using an inequality, rather than an equality, to allow inventory to reset to zero in time periods following start-up completion; inventory is naturally maximized by the problem and can only be nonzero for time steps in which the receiver is starting up by Constraint (2b). Constraint (2c) allows receiver power production only after start-up has been completed or when the receiver was operating in the previous time step. Constraint (2d) ensures that receiver start-up mode does not persist while the receiver is operating in power-producing mode by disallowing start-up in the time step following normal power production operation. Constraint (2e) ensures that the actual power used for receiver start-up is no more than the ramp rate limit for each time step. Constraint (2f) prevents receiver start-up from occurring in time periods with trivial solar resource.

The total power produced by the receiver has an upper bound of the available energy Q_t^{in}, and any start-up or shutdown energy consumption detracts from production according to Constraint (3a). The receiver can only generate thermal power when it is in power-producing mode (i.e., $y_t^r = 1$) by Constraint (3b). Constraint (3c) is enforced because of molten-salt pump operating limits and heat transfer requirements in the receiver, ensuring that the receiver energy generation must satisfy a minimum threshold. Constraint (3d) ensures that the receiver power-producing mode does not persist when no energy is available.

While the receiver is in standby mode, molten salt is circulated between the cold TES tank and receiver, enabling fast restart. A

Table 2
Variables used in ($\mathcal{R}$).

Symbol	Units	Description
Continuous		
x_t	kW_t	Cycle thermal power consumption at t
$\dot{w}_t$	kW_e	Electrical power generation at t
$\dot{w}_t^{\delta}$	kW_e	Positive change in electricity production at t
x_t^r	kW_t	Thermal power delivered by the receiver at t
x_t^{rsu}	kW_t	Receiver start-up power consumption at t
u_t^{rsu}	kW_t-hr	Receiver start-up energy inventory at t
u_t^{csu}	kW_t-hr	Cycle start-up energy inventory at t
s_t	kW_t-hr	TES reserve quantity at t (auxiliary variable)
Binary		
y_t^r		1 if receiver is generating "usable" thermal power at time t; 0 otherwise
y_t^{rsu}		1 if receiver is starting up at time t; 0 otherwise
y_t^{rsb}		1 if receiver is in standby mode at time t; 0 otherwise
y_t^{rsd}		1 if receiver shut down at time t; 0 otherwise
y_t^{csu}		1 if cycle is starting up at time t; 0 otherwise
y_t^{csb}		1 if cycle is in standby mode at time t; 0 otherwise
y_t^{csd}		1 if cycle is shutting down at time t; 0 otherwise
y_t		1 if cycle is generating electric power at time t; 0 otherwise
y_t^{rsup}		1 if receiver is starting up at time t and was not in standby mode at time $t-1$; 0 otherwise
y_t^{rhsp}		1 if receiver is starting up at time t and was in standby mode at time $t-1$; 0 otherwise
y_t^{csup}		1 if cycle is starting up at time t and was not in standby mode at time $t-1$; 0 otherwise
y_t^{chsp}		1 if cycle is starting up at time t and was in standby mode at time $t-1$; 0 otherwise

smaller hot start-up penalty is enforced when beginning normal operation from standby mode. Neither standby and start-up modes (Constraint (4a)) nor standby and power-producing modes (Constraint (4b)) can coincide. Standby mode can persist over time, but must follow time steps in which the receiver was either in standby or power-producing mode (Constraint (4c)). Constraints (4d) and (4e) enforce logic associated with incurring a penalty for receiver start-up from an off or standby state, respectively. Constraint (4f) enforces the logic for shut-down from a power producing or standby state. Constraint (10a) ensures non-negativity for receiver start-up power consumption and receiver start-up energy inventory. Non-negativity for x_t^r is ensured via Constraint (3c). Constraint (10c) enforces binary requirements on the variables associated with generating usable thermal power, receiver start-up, receiver standby, receiver shut down, and receiver start-up penalties.

2.4.2. Power cycle operations

Power cycle operation constraints largely mirror those of receiver operations and include:

Cycle Start-up

$$u_t^{csu} \leqslant u_{t-1}^{csu} + \Delta \cdot Q^c y_t^{csu} \quad \forall t \in \mathcal{T} : t \geqslant 2 \tag{5a}$$
$$u_t^{csu} \leqslant \mathbb{M} y_t^{csu} \quad \forall t \in \mathcal{T} \tag{5b}$$
$$y_t \leqslant \frac{u_t^{csu}}{E^c} + y_{t-1} + y_{t-1}^{csb} \quad \forall t \in \mathcal{T} : t \geqslant 2 \tag{5c}$$
$$x_t + Q^c y_t^{csu} \leqslant Q^u y_t \quad \forall t \in \mathcal{T} \tag{5d}$$
$$x_t \leqslant Q^u y_t \quad \forall t \in \mathcal{T} \tag{5e}$$
$$x_t \geqslant Q^l y_t \quad \forall t \in \mathcal{T} \tag{5f}$$

Power Supply and Demand

$$\dot{w}_t \leqslant \frac{\eta_t^{amb}}{\eta^{des}} (\eta^p x_t + y_t (W^u - \eta^p Q^u)) \quad \forall t \in \mathcal{T} \tag{6a}$$
$$\dot{w}_t^{\delta} \geqslant \dot{w}_t - \dot{w}_{t-1} \quad \forall t \in \mathcal{T} : t \geqslant 2 \tag{6b}$$

if $\dot{W}_t^{net} \geqslant \dot{W}_t^{min}$ then:

$$\dot{W}_t^{net} \geqslant \dot{w}_t (1 - \eta_t^c) - L^r (x_t^r + x_t^{rsu}) - x_t L^c - y_t^{rsu} \left(\frac{\dot{W}^{rsb}}{\Delta} + \frac{E^{hs}}{\Delta} \right) - \dot{W}^h y_t^r - y_t^{csb} \dot{W}^b \quad \forall t \in \mathcal{T} \tag{6c}$$

else:

$$\dot{w}_t = 0 \; \forall t \in \mathcal{T} \tag{6d}$$

Logic Governing Cycle Modes

$$y_t^{csu} + y_{t-1} \leqslant 1 \quad \forall t \in \mathcal{T} : t \geqslant 2 \tag{7a}$$
$$y_t^{csb} \leqslant y_{t-1} + y_{t-1}^{csb} \quad \forall t \in \mathcal{T} : t \geqslant 2 \tag{7b}$$
$$y_t^{csu} + y_t^{csb} \leqslant 1 \quad \forall t \in \mathcal{T} \tag{7c}$$
$$y_t + y_t^{csb} \leqslant 1 \quad \forall t \in \mathcal{T} \tag{7d}$$
$$y_t^{csup} \geqslant y_t^{csu} - y_{t-1}^{csu} \quad \forall t \in \mathcal{T} : t \geqslant 2 \tag{7e}$$
$$y_t^{chsp} \geqslant y_t - (1 - y_{t-1}^{csb}) \quad \forall t \in \mathcal{T} : t \geqslant 2 \tag{7f}$$
$$y_{t-1}^{csd} \geqslant (y_{t-1} - y_t) + (y_{t-1}^{csb} - y_t^{csb}) \quad \forall t \in \mathcal{T} : t \geqslant 2 \tag{7g}$$

Constraint (5a) tracks start-up energy inventory, and Constraint (5b) allows nonzero inventory only during periods of cycle start-up. Constraint (5c) allows normal cycle operation only when start-up has been completed, when the cycle was previously operating, or when the cycle has been in standby mode. Constraint (5d) limits the cycle start-up rate, and Constraint (5e) enforces a maximum thermal power consumption limit by the power cycle. When operating, the cycle must produce a minimum amount of power enforced by Constraint (5f). Constraint (6a) determines electrical power production based on a linear cycle performance curve and the ambient temperature efficiency. The positive change in electrical power production is determined by Constraint (6b). The presence of $\dot{w}_t^{\delta}$ in the objective function provides a disincentive to vary power production from one time step to the next, thereby reducing system cycling and more closely representing operator-preferred generation profiles. The appropriate magnitude of this penalty parameter is unknown but is explored further in a sensitivity analysis provided in Section 4. Constraints (6c) and (6d) ensure that if the net power production upper limit is greater than or equal to that of the lower limit in any given time period, then that former production level must exceed that actually produced when efficiency is accounted for, less that from parasitics due to pumping power, heliostat field start-up, heliostat field tracking, power cycle standby, and tower piping heat trace. If the net power production upper limit is less than the lower limit in any given time period, the production level is zero. Start-up mode persistence is prevented in Constraint (7a). Standby mode can persist according to the analogous receiver requirements (Constraint (7b)). Standby and start-up modes cannot coincide (Constraint (7c)), nor can standby and power-producing mode (Constraint (7d)). Constraint

(7e) enforces the penalty logic for start-up from an off state while (7f) enforces the penalty logic for start-up from a standby state. Constraint (7g) enforces the logic for shut-down from a power-producing or standby state. Constraint (10b) ensures non-negativity for cycle start-up energy inventory, electrical power generation, and positive change in electricity production. Non-negativity for x_t is ensured via Constraint (5f). Constraint (10d) enforces binary restrictions.

2.4.3. Energy balance

The energetic state of the system implicates positive and negative power terms, and the charge state of thermal storage (s_t) accounts for the cumulative difference between them. Several additional constraints regarding TES state of charge are enforced as follows:

$$s_t - s_{t-1} = \Delta \cdot [x_t^r - (Q^c y_t^{csu} + Q^b y_t^{csb} + x_t + Q^{rsb} y_t^{rsb})] \quad \forall t \in \mathcal{T} : t \geqslant 2 \tag{8a}$$

$$x_{t+1} + Q^b y_{t+1}^{csb} \leqslant \frac{s_t}{\Delta_{t+1}^{rs}} - \mathbb{M} \cdot (-3 + y_{t+1}^{rsu} + y_t + y_{t+1} + y_t^{csb} + y_{t+1}^{csb}) \quad \forall t \in \mathcal{T} : \; t \leqslant T - 1 \tag{8b}$$

Constraint (8a) ensures that energy into and out of TES balance with the charge state, and the conversion from power to energy introduces a time step parameter Δ. Constraint (8b) addresses an artifact arising from the difference between the modeling time resolution (hourly) and the amount of time required to start the plant, which may not be in units of whole hours. If the power cycle is either running or in standby in time step t and in time step $t+1$, and if the receiver starts up in time $t+1$, then the minimum charge level in TES in time $t+1$ must be sufficient to carry operation through the receiver start-up period. Note that $y_t + y_t^{csb} \leqslant 1$ is enforced elsewhere. Eq. (9) determines the expected fraction of each time step that would be used for receiver start-up, if applicable.

$$\Delta_t^{rs} = \min\left\{1, \max\left\{\Delta^l, \frac{E^c}{\max\left\{\epsilon, Q_{t+1}^{in}\Delta\right\}}\right\}\right\} \tag{9}$$

Constraints (8a)-(8b) only track TES state of charge based on energy flow bookkeeping, not temperature. Accounting for energy quality in the TES system via temperature of the molten salt introduces non-linear complexity and is not necessary in this formulation, as previously discussed.

Variable bounds are enforced in (10a)–(10d), with (10b) bounding both the minimum and maximum amount of energy in storage.

$$x_t^r, x_t^{rsu}, u_t^{rsu}, u_t^{csu} \geqslant 0 \quad \forall t \in \mathcal{T} \tag{10a}$$

$$x_t, \dot{w}_t^{\delta}, s_t \geqslant 0; \; s_t \leqslant E^u \quad \forall t \in \mathcal{T} \tag{10b}$$

$$y_t^r, y_t^{rsu}, y_t^{rsup}, y_t^{rsb}, y_t^{rhsp}, y_t^{rsd} \in \{0,1\} \quad \forall t \in \mathcal{T} \tag{10c}$$

$$y_t, y_t^{csu}, y_t^{csb}, y_t^{csup}, y_t^{chsp} \in \{0,1\} \quad \forall t \in \mathcal{T} \tag{10d}$$

2.4.4. Cycle part-load correction

An optimized dispatch profile may result in electricity production lower than the CSP plant design-point during certain time periods in order to conserve stored thermal energy for more favorable future market conditions, or to avoid penalties associated with shut-down and start-up, for example. However, power cycle efficiency is adversely affected by departure from design, as shown in Fig. 2 [28].

The relationship between thermodynamic efficiency and thermal input is nonlinear and, consequently, poses computational challenges. In order to improve tractability in the corresponding optimization model, an approximately linear function of cycle thermal power consumption resolves the nonlinearity $\eta^{cycle}(x_t) \cdot x_t$ by modeling *electrical output*, shown in Constraint (6a). The linear coefficient is the quotient of the difference between the minimum and maximum output from the power cycle and the corresponding expression for the thermal power input.

$$\eta^p = \frac{W^u - W^l}{Q^u - Q^l} \tag{11}$$

2.5. Dispatch model implementation

The typical model instance contains 912 variables and 1,615 constraints. AMPL and CPLEX presolve reductions result in a problem with an average of 442 variables and 652 constraints, and an average run time on a Dell PowerEdge R410 server running Ubuntu 14.04 with 12 GB RAM, 16 Intel processors at 2.72 GHz each of 0.43 s per 48-h horizon evaluation. By contrast, implementation of the model using LPSolve [29], which is a freeware MIP solver platform for C++, requires an average of 0.83 s per solve. Presolve reductions are less effective, producing instances with 890 variables and 920 constraints.

The number of time steps in the time horizon ($\mathcal{T}$) must be chosen with care, as it greatly affects the typical model described here as well as system techno-economic performance. The following considerations are relevant when choosing a time horizon duration: (i) the problem complexity grows exponentially with the time horizon length, and consequently, the amount of time needed for an annual simulation will also grow significantly; (ii) the opti-

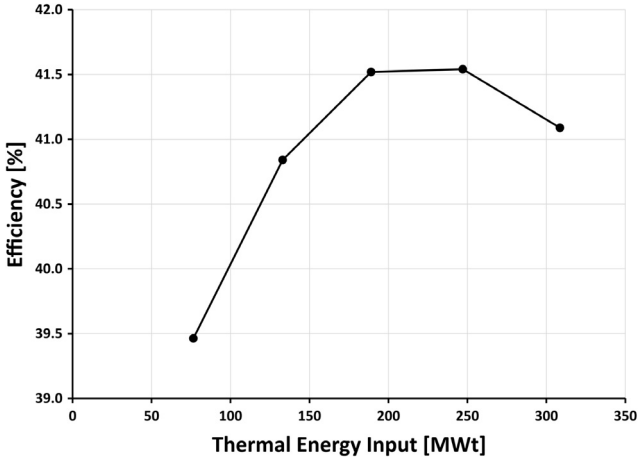

Fig. 2. Cycle efficiency as a function of input thermal power represented using a piece-wise linear function.

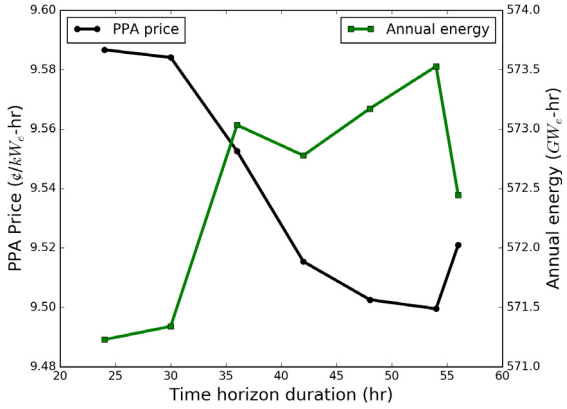

Fig. 3. The impact of time horizon length (hours) on annual energy production and PPA price.

Table 3
Case study plant design and control parameters.

Parameter	Units	Value
Gross electrical output	MW_e	115
Cycle design efficiency	%	41.2
Cycle design thermal input	MW_t	278.1
Cycle maximum output	MW_e	120.75
Cycle minimum output	MW_e	28.75
Cycle start-up energy	MW_t-hr	57.5
Cycle start-up time	hr	0.5
Cycle standby consumption	MW_t	23
Receiver max. output (relative*)	–	1.2
Receiver min. output (relative)	–	0.25
Receiver start-up energy (relative)	–	0.25
Receiver start-up time (relative)	–	0.2
Receiver HTF temperature	°C	574
Heat rejection technology	–	Air cooled
Heliostat size	m^2	144.4
Maximum receiver flux	kW/m^2	1,000
Hours of TES	hr	1,...,18
Solar multiple	–	0.8,...,3

* Relative to receiver thermal input design point.

mized dispatch profile maximizes revenue within the allotted time horizon, and an insufficiently long horizon emphasizes near-term production at the expense of future, higher-value time periods; (iii) an optimal profile may require thermal energy to be held in storage overnight, and an insufficiently long time horizon (e.g., 24 hours) will fail to account for next-day requirements; and, (iv) given limitations on the number of branch-and-bound iterations and/or computation time per solve, an increased horizon length raises the likelihood of adopting a suboptimal dispatch profile, thereby negatively affecting expected plant performance. Fig. 3 shows the impact of the time horizon length on the annual energy production and power purchase agreement (PPA) price (discussed in the next section) for the reference plant defined in Table 3.

3. Model implementation

Fig. 4 illustrates the dispatch optimization model within SAM whose interface provides both input and output display. The user selects the technology and financial model, then modifies the inputs to emulate their technology configuration of interest, after which SAM simulates technical and financial performance by sending information from the interface to the SAM Simulation Core. Therein lies the molten salt power tower (MSPT) technology model that contains a solar field design algorithm called SolarPILOT and detailed calculators for determining weather data and the performance of the collector, receiver, power block, and TES subsystems.

The MSPT model simulates annual production by evaluating performance over a sequence of hourly time steps, at each of which the *CSP controller* determines the best operational mode given the conditions endogenous and exogenous to the system. The *CSP solver* ensures that all of the interconnected inputs and outputs among the calculators agree with respect to the thermodynamic state of the system. In summary, the architecture in Fig. 4 characterizes a molten salt power tower plant with storage, in which the hour-by-hour plant operation protocol is determined using a 48-h time horizon that rolls forward in 24-h increments.

The *Production Forecast Model* determines expected future thermal energy generation of the solar field. While it is possible to implement a variety of techniques for predicting electricity pricing, ambient temperature, and direct normal irradiance, this paper uses "perfect forecasting" in which the model generates expected performance by reading ahead in the weather file. MSPT incorporates the time series data from the weather and pricing databases corresponding to the horizon over which the model is solved.

The heliostat field concentrates power on the receiver (Q_t^{helio}) according to the instantaneous optical efficiency (η_t^{sf}), direct normal irradiance (d_t), and mirror area (A^{sf}).

$$Q_t^{helio} = \eta_t^{sf} d_t A^{sf} \tag{12}$$

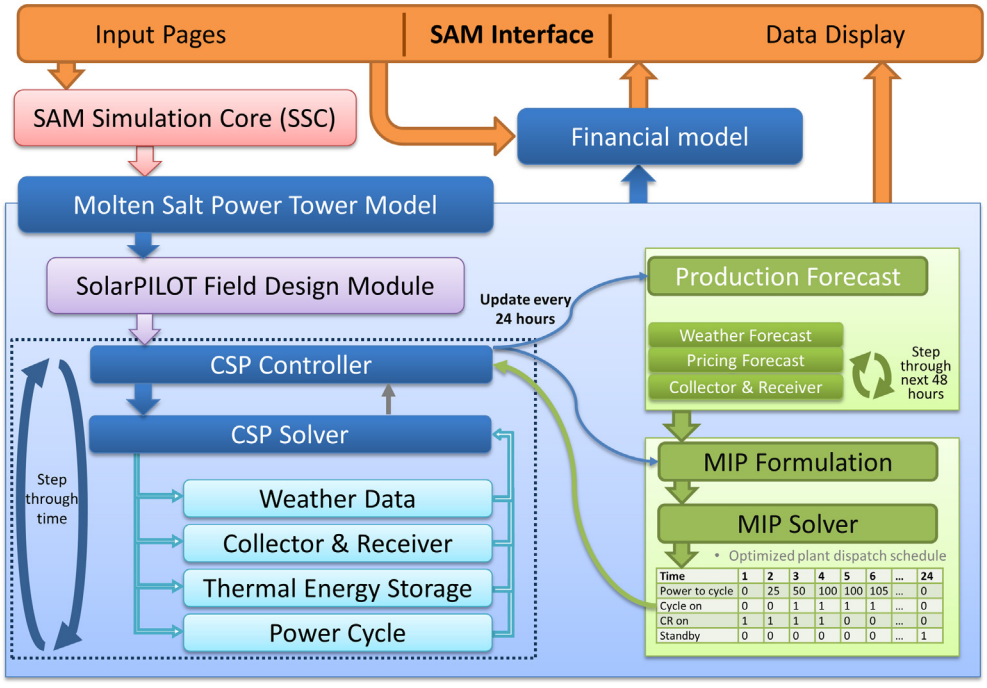

Fig. 4. Information flow in the MSPT model. The MIP formulation is solved as a simultaneous set of equalities and inequalities, and the hourly solution profile is used by the CSP controller to set target power production levels and operational states over the subsequent operational time horizon.

The total expected solar field production is the nonnegative difference of incident power on the receiver and convective (Q_t^{conv}) and radiative (Q_t^{rad}) thermal losses:

$$Q_t^{in} = \max\left[0, Q_t^{helio} - Q_t^{conv} - Q_t^{rad}\right] \quad \forall t \in \mathcal{T} \tag{13}$$

The following reduced-order relationships model the expected technical performance of the collector and receiver, providing a reasonably accurate approximation of expected field productivity. The collector field model generates a lookup table containing optical efficiency as a function of sun position, and the CSP controller supplies this information to the forecast model. The complexity of modeling the receiver thermal loss via convection and radiation from the heated surface necessitates a simplified forecasting model: an area-weighted average molten salt temperature is given as the weighted average of the inlet and outlet temperatures, where the coefficient is receiver-specific [30].

$$T^{eff} = 0.55 \cdot (T^{out} + T^{in}) \tag{14}$$

Radiative losses are calculated at each time t as:

$$Q_t^{rad} = A^{rec}\sigma\epsilon\left((T^{eff})^4 - (T_t^{amb})^4\right) \tag{15}$$

in which A^{rec} is the receiver surface area, σ is the Stefan-Boltzmann constant, ϵ is the temperature-weighted surface emittance, and T_t^{amb} is the expected ambient dry-bulb temperature. Convective losses are expressed as a function of wind velocity for the molten salt technology, scaled by radiative loss. The coefficients in (16) are determined by regressing simulated data points that are generated using the MSPT detailed receiver model.

$$Q_t^{conv} = \left(-5.645 \times 10^{-4} V_t^3 + 0.01561 V_t^2 - 0.00911 V_t + 0.48124\right) Q_t^{rad} \tag{16}$$

where V_t is the wind velocity at time t.

The Engineering Performance Model (consisting of the CSP controller, CSP solver, and detailed performance calculators in Fig. 4) predicts plant behavior and productivity over time using computationally expensive procedures derived from physically based, first-principles modeling of thermodynamics and heat transfer phenomena. The model's engineering performance behavior is validated and discussed in detail in [28,31].

The MIP Mathematical Formulation, when solved with an appropriate algorithm, determines the performance and operation of the plant using the forecast model and various operational constraints (see Section 2).

The Pricing Model calculates the PPA price, which is the minimum value at which a power producer should agree to sell electricity in order to ensure that a specified internal rate of return is achieved. The PPA price is a useful surrogate for the profitability of a project in that it accounts for the variability in electricity value with time of day and time of year. As it is applied in SAM, the PPA price is multiplied by the hour-by-hour TOD or "tariff" rate to determine the value of electricity generated by the plant over time. SAM calculates the PPA price assuming a target internal rate of return (11% in the current study) and an annual escalation rate of 1%. For this reason – and somewhat counter-intuitively – a low PPA price is desirable. From the perspective of a power producer, a low PPA price improves its competitiveness. Alternatively, the PPA price could be specified and the internal rate of return maximized, and results from either approach would be equivalent. The results here translate the objective function value of ($\mathcal{R}$) into PPA price by taking fixed costs as sunk and maximizing revenue generated from electricity sales.

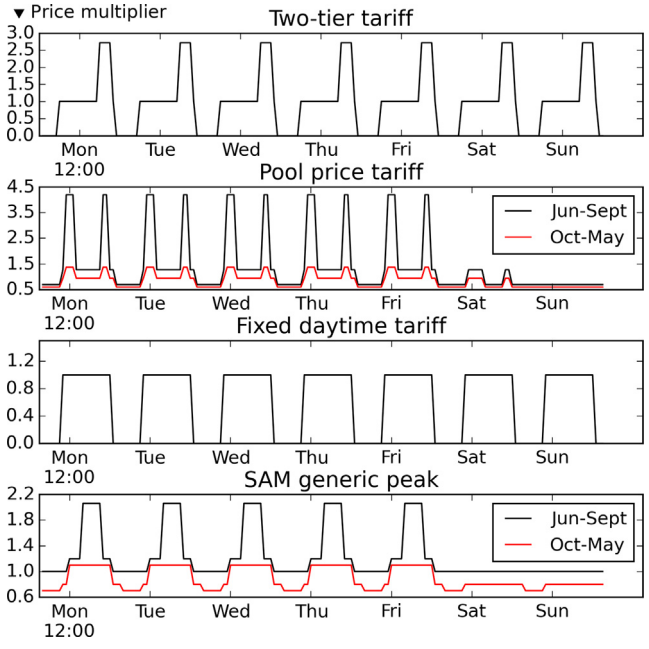

Fig. 5. Market pricing scenarios presented by Guédez et al. [22]. These tariff schedules are implemented to determine the impact of dispatch optimization on system sizing.

4. Case studies

This study explores a range of plant TES sizes and solar multiples, the latter of which is defined as the ratio of solar field thermal power output to power cycle thermal input at design conditions. As the solar multiple increases, so too does the optimal amount of TES and the resulting plant capacity factor, but these values may be chosen independently. Table 3 provides a summary of key design parameters which are obtained from the default SAM-MSPT case. For this analysis, SAM automatically determines the heliostat field layout given the specified solar multiple and other design parameters. Each evaluation takes as fixed the TES and solar multiple and determines the optimal dispatch schedule for that system configuration.

In addition, this analysis considers four market scenarios (Fig. 5), three of which have been adopted from [22], and one of which is the "generic summer peak" scenario used as the default for the MSPT model. The two-tier tariff market encourages daytime production with an evening spike. The pool price tariff introduces an additional morning spike and weights incentives seasonally. The fixed daytime tariff allows sales during daytime hours, but is unique in its binary nature; no revenue is available during nighttime operation. Finally, the SAM generic peak schedule combines features from the two-tier and pool price tariffs.

Using MSPT, this paper compares the dispatch optimization methodology to the previous approach that relies on heuristic control which was configured to allow power generation any time the TES state of charge exceeded the threshold for minimum power cycle operation (satisfying Constraint (5f)). The cycle generates power at the design-point level unless insufficient energy is available in storage. Power cycle start-up occurs whenever energy in storage exceeds the quantity needed to deliver the start-up power for a single time period. The heuristic allows power generation until energy storage is exhausted each night, if applicable. This approach emphasizes maximum energy generation throughout the year.

4.1. Results

Table 4 presents the results of the PPA analysis, where the reported values correspond to the configuration with the

Table 4
Characteristics for each market scenario in which PPA price is at a minimum value, both for heuristic (H) and optimized (O) dispatch.

Market scenario	Solar mult.		Hours TES		PPA price	
	H	O	H	O	H	O
Two-tier	2.2	2.0	5	7	8.97	7.71
Pool price	2.2	2.2	8	9	9.66	8.75
Fixed daytime	1.8	2.0	4	6	13.30	12.75
SAM default	2.6	2.6	12	14	10.41	10.09

minimum PPA price for the indicated scenario. Dispatch optimization successfully reduces PPA price compared to the heuristic dispatch method. Heavily weighted schedules (i.e., pool price and two-tier) lead to more substantial PPA price reductions (about 10–15%), indicating that dispatch optimization is an essential aspect of plant operation for "peaker" markets that provide relatively short time windows of high-value energy pricing. The reader can also observe that systems operating in markets with more uniform tariff factors still benefit significantly from dispatch optimization, which alters the size of TES and the solar multiple at which PPA price is minimized. This implies that dispatch optimization should not be relegated to operational analyses, but rather should be part of the project screening and design process.

An important feature of dispatch optimization is the apparent improvement in the consistency of production during high-value time periods. Fig. 6 illustrates this behavior for the pool price tariff scenario. Figs. 6a and b show the hourly TES charge state profiles for each day of the year for both heuristic and optimized dispatch, respectively. Also shown on the plot are the tariff multiplier schedules for summer (black) and winter (green) that determine the revenue associated with generation during a particular hour of the day.

Dispatch optimization substantially changes the daily operational profile. Whereas heuristic dispatch allows TES to discharge in the evening and late-night hours, optimized dispatch typically reserves some quantity of TES to allow morning start-up. The TES profiles show that heuristic dispatch is much more operationally repetitive relative to optimized dispatch, implying that the latter strategy accounts for expected resource availability and future pricing when scheduling TES usage.

Figs. 6c and d show the distribution of electricity generation for each hour of the day over the course of the year. Each box-whisker plot describes the variability in electricity generation for each day at the specified hour, and the box limits indicate the extents of the first and third quartiles. The whiskers correspond to twice the inner quartile range. Points that lie outside of this limit are plotted individually and are distribution outliers.

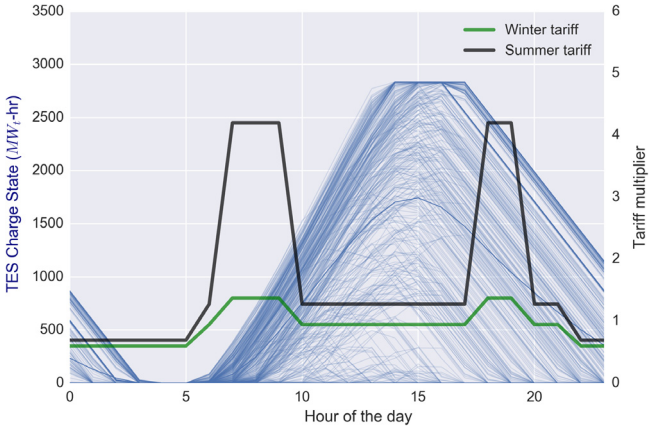

(a) Daily thermal storage charge state profile - **heuristic** dispatch

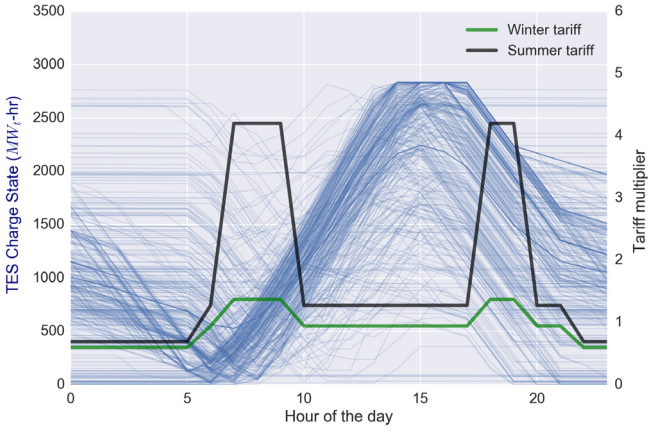

(b) Daily thermal storage charge state profile - **optimized** dispatch

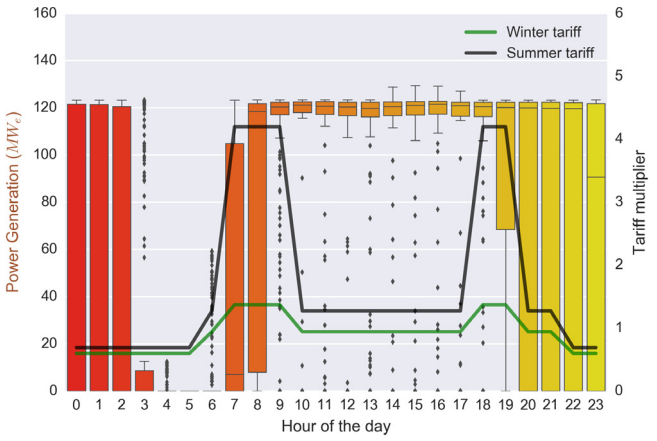

(c) Annual variability of electricity generation - **heuristic** dispatch

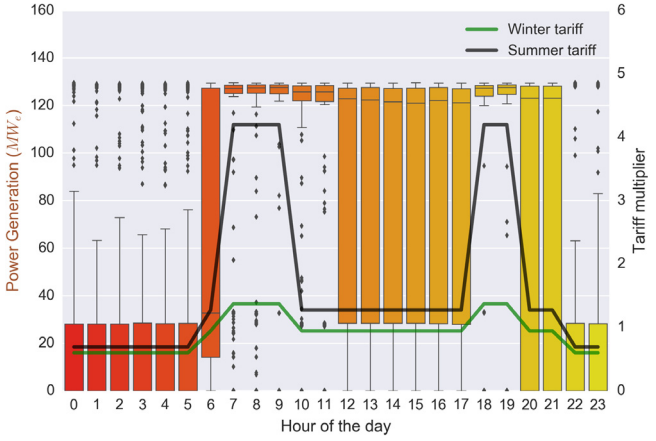

(d) Annual variability of electricity generation - **optimized** dispatch

Fig. 6. Comparison of performance profiles for the pool price tariff schedule. Plots (a) and (b) show traces of the TES charge state for each day of the year. Plots (c) and (d) show box-whisker plots of daily electricity production variability over a year grouped by hour of the day. Each box indicates the mean annual electricity generation by hour, the first and third quartile limits (box limits), and two times the interquartile range (whiskers). "Outliers" are shown as black dots. Summer (black) and winter (green) tariff multipliers are overlaid on each plot. (For interpretation of the references to color in this figure legend, the reader is referred to the web version of this article.)

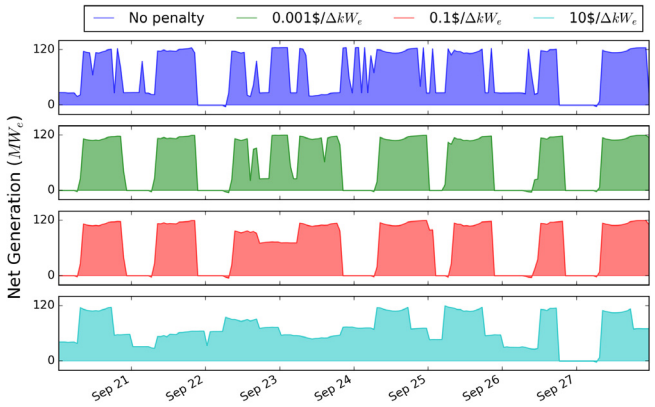

Fig. 7. Plant power generation profile with varying change in production penalty values, $C^{\delta \dot{W}}$. (Penalties are given in the legend.)

Fig. 6c shows that heuristic electricity production is highly variable in the early morning, evening, and nighttime hours (tall boxes) and is less variable during daytime hours (short boxes). The variability in electricity generation is inversely related to solar resource availability – an intuitive observation. However, production is highly variable during peak revenue hours as shown by the tariff multipliers. Fig. 6d depicts optimized dispatch in which electricity generation variability is reduced during peak revenue hours.

4.2. Penalty parameter sensitivity study

This study also seeks to understand the impact of operational cost parameters on both the generation profile and on PPA price. Plant operation that requires multiple daily start-ups or frequent production ramping may be difficult to execute and lead to additional maintenance costs over time. This paper quantifies the revenue and production impact of obtaining "desirable" operational profiles (that is, relatively consistent output with few starts or ramp events).

The production change penalty, $C^{\delta \dot{W}}$, penalizes any *positive* change in power cycle electricity production from one hour to the next. Fig. 7 presents the dispatch profile over several selected days in September in which four different penalty values are used. As the value of $C^{\delta \dot{W}}$ increases, the optimal solution sacrifices maximizing generation during periods of peak revenue and cycle efficiency to improve output stability. If increased to an extreme ($C^{\delta \dot{W}} = 10.0$), the dispatch profile approaches that of a baseload plant, only peaking for very short periods of time.

This analysis leads to several considerations regarding the optimal design of a CSP plant given the potential ramping costs of the cycle. Namely, if production change costs truly are on the order of $10\$/\Delta kWe$, then the solar multiple, thermal storage, and power cycle sizes should generally be chosen to mimic a baseload plant. Penalties for frequent production changes would only be offset for the case in which TOD pricing variations are very large. Furthermore, an operator might reduce dispatch profile complexity but at some expense to apparent near-term plant profitability.

This paper also considers two TOD pricing scenarios ("Default" and "Peaker") in which the hours of TES and solar multiple are optimized for the no-penalty case. The first scenario is the generic summer peak profile in SAM, and the second is the pool price profile with spikes in pricing in the morning and evening and a price reduction during the middle of the day.

Fig. 8 shows the impact of increasing the production change cost penalty on annual energy generation, PPA price, and number of turbine cycles per day, which is calculated as the total annual positive change in cycle production normalized to a value that corresponds to ramping the cycle from off to full load once a day for the entire year. If the number of cycles per day is greater than unity, then the turbine experiences more than one full cycle per day on average.

Several interesting observations arise from this analysis. First, the number of cycles per day decreases as the production change cost penalty increases, as intended. If production variability is not penalized at all, the optimal solution results in more than one cycle on average per day for both the Default and Peaker cases. As the penalty for changing production increases, the number of cycles drops significantly, which may be an important factor in increasing plant lifetime and reducing maintenance costs. Remarkably, the number of cycles can be reduced by 50% or more by manipulating this penalty without significant degradation of the objective function value.

Second, the trends in reduction of cycles per day, annual energy generation, and PPA price are mirrored between the Default and Peaker cases. Both show that production change cost in the range of 0.5–2.0 $\$/kW_e$ minimizes PPA price and number of cycles per day, though the true costs of turbine ramping are not known and thus omitted from the PPA calculation. Non-coincidence of this

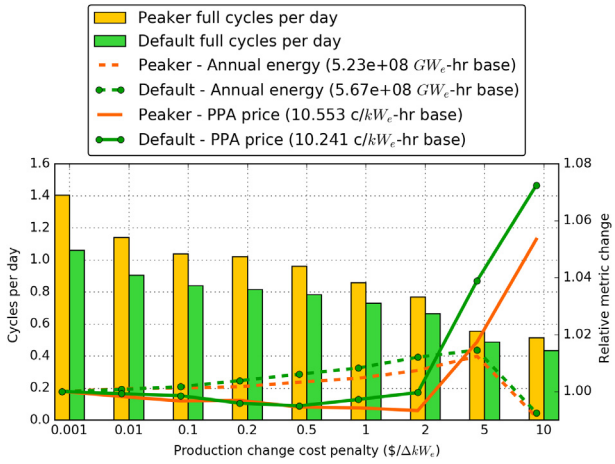

Fig. 8. Impact of production change cost penalty on the number of turbine cycles per day, annual energy generation, and PPA price for two pricing scenarios – a generic summer afternoon peak schedule (Default) and a morning/evening double-peak (Peaker) schedule. Annual energy and PPA price are shown as fractional values relative to the lowest-penalty case.

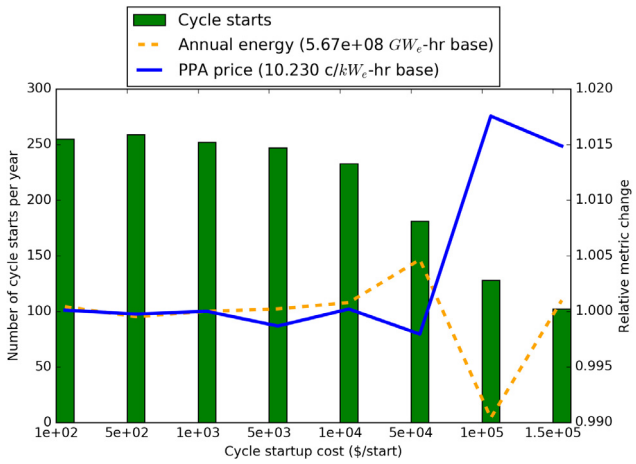

Fig. 9. Number of cycle starts per year, annual energy output, and PPA price for the Default case with varying scenarios for cycle start-up cost.

outcome may imply an important cost threshold regarding CSP plants in general. Lastly, increasing the penalty leads to reduced annual output and increased PPA price below a threshold corresponding to 0.4–0.6 cycles per day.

A final study considers the cycle start-up cost penalty's impact on the same performance metrics. This penalty is related to ramping cost, but differs in that it represents a penalty incurred for a discrete event that occurs only when the power cycle transitions from an *off* state to an *on* state, after which this penalty does not influence operation. Fig. 9 shows the result of varying start-up cost for the Default case.

As with the production change penalty, the start-up penalty can significantly affect the behavior of the power cycle. A small cost of $100 per start leads to a relatively large annual number of cycle starts (about 250). As a point of comparison, the number of cycle starts incurred using heuristic dispatch is 370 per year. The number of starts remains fairly constant (within variance that is to be expected based on numerical error in the solution) until the cost increases by a factor of 100, and a factor increase of 1,000 reduces starts by approximately 50% without a significant effect on annual energy output and PPA price. Therefore, operational protocols that seek to minimize full cycle starts and stops can theoretically offer equally viable financial performance compared to more traditional approaches.

4.3. Applications

The results shown herein are readily applicable in practice, both for modeling and plant operations applications. First, modeling activities are fundamental to research, project development, and policymaking decisions, and an accurate estimate of technology performance directly impacts each of these areas. Researchers require tools that quantify the impact of advances in the technology, and utilize models to identify research priorities. The provision of a dispatch optimization tool in a publicly available software package enables assessment of the value of new thermal energy storage technologies – e.g., [32], or power cycles – e.g., [33], that otherwise may not interact with other subsystems as anticipated upon deployment. Project developers rely on models for initial plant design, attaining financing, project permitting, and finally, during plant operation. Dispatch optimization tools such as this are valuable for these purposes, and the authors present additional applied results and model validation in [34].

5. Conclusions

This paper develops and implements a mixed-integer programming model within SAM to optimize the TES dispatch schedule for a molten salt power tower plant; this schedule provides a target power generation profile that is used in conjunction with a simulation model that evaluates plant performance at an hourly level over a year-long time horizon. SAM's detailed performance model mitigates some of the approximations present in the MIP formulation.

The results indicate that dispatch optimization can significantly improve plant revenue, though the gains vary with plant capacity factor and electricity markets. In particular, scenarios with heavily weighted pricing schemes or narrow windows of high revenue benefit the most, e.g., PPA price (indicative of the profitability of the plant), can improve by 10–15%. Plant revenue is negatively affected by the energetic and financial cost of starting the solar receiver and power cycle equipment, and this paper shows that optimized generation profiles can achieve a reduction in the number of turbine starts per year by 50% or more – in some circumstances – with little impact on project financial performance.

In summary, this model provides a methodology to optimize the trade-offs between CSP component and subsystem performance, the effects of demand, and the amount of revenue obtained under various market schedules. Future work will incorporate, inter alia, forecast uncertainty, and more precise cost estimates of component operations and maintenance requirements. It will also examine how plant design and maintenance affect the overall cost and nature of the dispatch strategy.

Acknowledgments

This work was funded by the United States Department of Energy – Energy Efficiency and Renewable Energy under award numbers DE-EE00025831 and DE-EE00030338. The authors gratefully acknowledge Jennifer DiCarlo at Colorado School of Mines for her contributions to the MIP mathematical formulation, Mark Mehos at the National Renewable Energy Laboratory for guidance on market factors, and Charles Diep and Jolyon Dent at SolarReserve® for feedback on modeling priorities and plant operations.

References

[1] Margolis R, Coggeshall C, Zuboy J. Sunshot vision study. US Dept. of Energy, February.
[2] Gil A, Medrano M, Martorell I, Lázaro A, Dolado P, Zalba B, Cabeza LF. State of the art on high temperature thermal energy storage for power generation. Part 1-Concepts, materials and modellization. Renew Sustain Energy Rev 2010;14(1):31–55.
[3] Jorgenson J, Denholm P, Mehos M. Estimating the value of utility- scale solar technologies in California under a 40% renewable portfolio standard. Tech. rep. May. Golden, CO: National Renewable Energy Laboratory; 2014.
[4] Turchi C, Mehos M, Ho CK, Kolb GJ. Current and future costs for parabolic trough and power tower systems in the US market preprint. Renew Energy 2010(October):11.
[5] Dunn RI, Hearps PJ, Wright MN. Molten-salt power towers: newly commercial concentrating solar storage. Proc IEEE 2012;100(2):504–15.
[6] Burgaleta JI, Arias S, Ramirez D. Gemasolar: the first tower thermosolar commercial plant with molten salt storage system. In: SolarPACES conference.
[7] Herrmann U, Kelly B, Price H. Two-tank molten salt storage for parabolic trough solar power plants. Energy 2004;29(5–6):883–93.
[8] Denholm P, Mehos M. Enabling greater penetration of solar power via the use of CSP with thermal energy storage. Tech. rep. November, Golden, CO; 2011.
[9] Pruitt KA, Braun RJ, Newman AM. Evaluating shortfalls in mixed-integer programming approaches for the optimal design and dispatch of distributed generation systems. Appl Energy 2013;102:386–98.
[10] Blair N, Dobos AP, Freeman J, Neises T, Wagner M, Ferguson T, Gilman P. System advisor model, SAM 2014.1.14: general description. Tech. rep. February, National Renewable Energy Laboratory, Golden, CO; 2014.
[11] National Renewable Energy Laboratory, System Advisor Model; 2012.
[12] Perera A, Attalage R, Perera K, Dassanayake V. A hybrid tool to combine multi-objective optimization and multi-criterion decision making in designing standalone hybrid energy systems. Appl Energy 2013;107:412–25.
[13] Nosrat A, Pearce JM. Dispatch strategy and model for hybrid photovoltaic and trigeneration power systems. Appl Energy 2011;88(9):3270–6.
[14] Pandžić H, Kuzle I, Capuder T. Virtual power plant mid-term dispatch optimization. Appl Energy 2013;101:134–41.
[15] Martinez-Rojas M, Sumper A, Gomis-Bellmunt O, Sudrià-Andreu A. Reactive power dispatch in wind farms using particle swarm optimization technique and feasible solutions search. Appl Energy 2011;88(12):4678–86.
[16] Thorin E, Brand H, Weber C. Long-term optimization of cogeneration systems in a competitive market environment. Appl Energy 2005;81(2):152–69.
[17] Cho H, Mago PJ, Luck R, Chamra LM. Evaluation of CCHP systems performance based on operational cost, primary energy consumption, and carbon dioxide emission by utilizing an optimal operation scheme. Appl Energy 2009;86(12):2540–9.
[18] Fürsch M, Hagspiel S, Jägemann C, Nagl S, Lindenberger D, Tröster E. The role of grid extensions in a cost-efficient transformation of the European electricity system until 2050. Appl Energy 2013;104:642–52.
[19] Parisio A, Rikos E, Tzamalis G, Glielmo L. Use of model predictive control for experimental microgrid optimization. Appl Energy 2014;115:37–46.
[20] Zheng Y-J, Chen S-Y, Lin Y, Wang W-L. Bio-inspired optimization of sustainable energy systems: a review. Math Problems Eng 2013.
[21] Hirsch T, Blanco MJ, Feldhoff JF, Eck M, Wagner MJ. Standardization of CSP performance model projection latest results from the stamp project. In: Proceedings of the ASME 2011 international conference on energy sustainability. p. 1–6.
[22] Guédez R, Ferragut F, Défense PL, Topel M, Callaba I, Pérez-Segarra CD. A methodology for determining optimum solar tower plant configurations and operating strategies to maximize profits. In: Proceedings of the ASME 2015 9th

international conference on energy sustainability. San Diego, CA: American Society of Mechanical Engineers. p. 1–15.
[23] Fourer R, Gay D, Kernighan B. AMPL, vol. 119. Boyd & Fraser; 1993.
[24] IBM. IBM ILOG CPLEX V12.1 user's manual for CPLEX; 2009.
[25] Madaeni SH, Sioshansi R, Denholm P. How thermal energy storage enhances the economic viability of concentrating solar power. Proc IEEE 2012;10 (2):335–47.
[26] Sioshansi R. The value of concentrating solar power and thermal energy storage. IEEE Trans Energy 2010;1(3):173–83.
[27] Guédez R, Spelling J, Laumert B, Fransson T. Reducing the number of turbine starts in concentrating solar power plants through the integration of thermal energy storage. In: Proceedings of the ASME turbo expo 2013, San Antonio, Texas. p. 1–10.
[28] Wagner MJ. Simulation and predictive performance modeling of utility-scale central receiver system power plants [Masters thesis]. Madison: University of Wisconsin; 2008.
[29] Berkelaar M, Eikland K, Notebaert P. LPSolve: open source (mixed-integer) linear programming system. Eindhoven U. of Technology.
[30] Lata JM, Rodríguez M, de Lara MÁ. High flux central receivers of molten salts for the new generation of commercial stand-alone solar power plants. J Sol Energy Eng 2008;130(2):021002.
[31] Wagner MJ, Gilman P. Technical manual for the SAM physical trough model, Tech. rep. June. Golden, CO: National Renewable Energy Laboratory; 2011.
[32] Singh D, Zhao W, Yu W, France DM, Kim T. Analysis of a graphite foam-NaCl latent heat storage system for supercritical CO_2 power cycles for concentrated solar power. Sol Energy 2015;118:232–42.
[33] Neises T, Turchi C. A comparison of supercritical carbon dioxide power cycle configurations with an emphasis on CSP applications. Energy Proc 2014;49:1187–96.
[34] Wagner MJ, Newman A, Braun R, Dent J, Diep C. Dispatching power at a concentrated solar energy facility. Working paper.